Journal of Materials Chemistry

Cite this: J. Mater. Chem., 2012, 22, 8372

www.rsc.org/materials

PAPER

Graphene–nanowire hybrid structures for high-performance photoconductive devices†

Hyungwoo Lee,‡[a] Kwang Heo,‡[b] Jaesung Park,[c] Yongju Park,[d] Seunguk Noh,[d] Kwang S. Kim,[c] Changhee Lee,[d] Byung Hee Hong,[e] Jikang Jian*[f] and Seunghun Hong*[abg]

Received 13th December 2011, Accepted 17th February 2012
DOI: 10.1039/c2jm16565a

Graphene–CdS nanowire (NW) hybrid structures with high-speed photoconductivity were developed. The hybrid structure was comprised of CdS NWs which were selectively grown in specific regions on a single-layer graphene sheet. The photoconductive channels based on graphene–CdS NW hybrid structures exhibited much larger photocurrents than graphene-based channels and much faster recovery speed than CdS NW network-based ones. Our graphene–CdS NW structures can be useful because they were much faster than commercial CdS film-based photodetectors and had photocurrents large enough for practical applications.

Introduction

The photoconductivity effect in various semiconducting materials has been a key for various optoelectronic circuits.[1–4] For example, the photoconductive channels based on bulk CdS films have been extensively utilized to build commercial photoconductive channel devices whose main advantage is that their resistance is linearly proportional to the intensity of the incident lights.[2] However, in previous photoconductive channels, the generated electrons and holes survive for a rather long time period like a few milliseconds even after the lights are turned off, resulting in a long response time to external light pulses.[2,3] For example, the commercial photoconductive devices based on CdS films usually have a response time of a few milliseconds. On the other hand, the devices based on semiconducting nanowires (NWs) as a photoconductive channel have been reported to have improved photoresponses and efficiencies compared with those based on bulk films.[5–11] Especially, a lot of efforts have been devoted to improve the performance of NW-based photoconductive channels using individual NWs.[12–16] However, the complex and time-consuming assembly of a single NW hinders practical applications. Recently, single-layer graphene (SLG) was reported to have a fast photoconductivity.[17,18] However, the photoconductive current in SLG is quite small[19] and, thus, the optoelectronic applications of SLG seem to have a long way to go.

Herein, we report graphene–CdS NW hybrid structures for high-speed photoconductivity and rather large photocurrents. The hybrid structure was comprised of CdS NWs which were selectively grown in specific regions on a SLG sheet. The photoconductive channels based on such graphene–CdS NW hybrid structures exhibited rather high photocurrent as well as much faster operation speed than those based on CdS NW networks.[8] This hybrid structure can be useful for practical applications because they were much faster than commercial CdS film-based photodetectors and exhibited photoresponses large enough for practical applications. This simple but efficient strategy allows us to take advantages of both graphene and NWs, and it should enable high performance optoelectronic devices for practical applications.

Experimental

Fabrication process of photoconductive channels based on graphene–CdS NW hybrid structures

Fig. 1 shows schematic diagrams depicting the fabrication method and operating principle of our photoconductive channels based on graphene–CdS NW hybrid structures. First, a SLG sheet was transferred onto a SiO_2 substrate as reported previously (Fig. 1a).[20,21] Then, an 8 nm thick Au film was deposited as a catalyst in the specific region of the graphene surface using a shadow mask (Fig. 1b). Subsequently, single-crystalline CdS NWs were grown selectively on the catalyst patterns of the

[a]Department of Physics and Astronomy, Seoul National University, Seoul, 151-747, Korea
[b]Interdisciplinary Program in Nano-Science and Technology, Seoul National University, Seoul, 143-747, Korea
[c]Department of Chemistry, Pohang University of Science and Technology, Pohang, 790-784, Korea
[d]School of Electrical Engineering and Computer Science, Seoul National University, Seoul, 151-747, Korea
[e]Department of Chemistry, Seoul National University, Seoul, 151-747, Korea
[f]School of Physical Science and Technology, Xinjiang University, Xinjiang 830046, P.R. China. E-mail: jianjikang@sina.com
[g]Department of Biophysics and Chemical Biology, Seoul National University, Seoul, 151-742, Korea. E-mail: seunghun@snu.ac.kr
† Electronic supplementary information (ESI) available: Experimental procedures and supplementary figures. See DOI: 10.1039/c2jm16565a
‡ These authors contributed equally to this work.

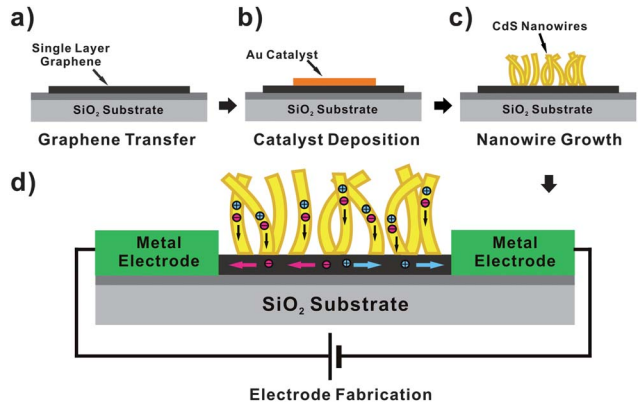

Fig. 1 Schematic diagram depicting the fabrication process of high-performance photoconductive channels based on graphene–CdS NW hybrid structures. (a) Transferring of a single-layer graphene sheet onto a SiO_2 substrate. (b) Deposition of an Au catalyst layer on the graphene. (c) Growth of CdS NWs on the Au catalyst using a vacuum furnace. Here, CdS NWs were grown only in the region of the patterned Au catalyst. (d) Fabrication of metal electrodes which were deposited on the both edges of a graphene sheet. Note that the light increased carriers in the NWs, and graphene transferred the carriers to the electrodes.

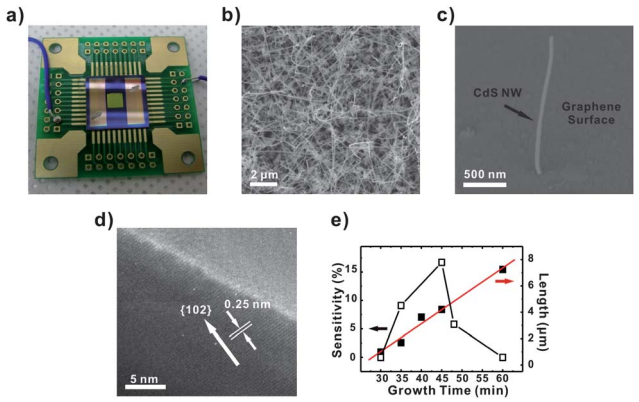

Fig. 2 CdS NWs on graphene. (a) Optical image of a photoconductive channel based on graphene–CdS NWs hybrid structures. (b) SEM image of the CdS NWs on graphene. The NWs were grown for 45 minutes. (c) SEM image showing the interface between a single CdS NW and the graphene surface. (d) HRTEM image of an as-grown CdS NW. This image reveals the single crystalline wurtzite structure of our CdS NWs. (e) Averaged length of NWs and the sensitivity of the photoconductive channels with various growth times. The length of the NWs increased linearly as the growth time increased. The sensitivity of our photoconductive channels increased as the growth time was increased up to 45 minutes, while it decreased when the growth time was increased over 45 minutes.

graphene sheet in a horizontal tubular furnace *via* the method similar to previous works.[5,22,23] The furnace includes an aluminium oxide (alumina) tube and a small alumina pot filled with a CdS source (Alfa Aesar, purity 99.99%, <44 μm) in the uniform temperature zone of the tube (Fig. 1c). Here, we placed the SLG sheet with the catalyst patterns on the downstream position of the source materials and kept the furnace at 650 °C for 45 minutes unless specified otherwise. The length of the NWs could be controlled by changing the growth time. Lastly, metal electrodes (Ti/Au) were fabricated by thermal evaporation through the shadow mask. Fig. 1d shows the final photoconductive channel device and a plausible mechanism for its photocurrent generation. When the photoconductive channel is exposed to light, electron–hole pairs are generated in the semiconducting CdS NWs.[5,22,23] These photo-generated charge carriers flow in the graphene channels *via* the applied bias voltage resulting in the photocurrents.

Results and discussion

Selective growth of CdS NWs on the graphene surface

Fig. 2a shows the optical image of our device on a PCB board. The length of graphene channel was 5 mm, and the CdS NWs were grown in a 4 × 4 mm^2 square region in the middle of the graphene channel. By patterning the catalyst, the selective growth of NWs could be achieved since the CdS NWs grew only in the patterned Au catalyst region (Fig. S1 in the ESI†). Metal electrodes were connected to a commercial PCB board by Au wire bonding. We used silver paste to reduce the contact resistance between the electrodes and the Au wires.

Fig. 2b shows the scanning electron microscopy (SEM) image of graphene–CdS NW hybrid structures in the fabricated photoconductive channel. The CdS NWs were grown in random orientations just like previous results on other substrates.[5,22,23] The high resolution SEM image of individual CdS NWs shows that the CdS NWs made a direct contact with the graphene surface (Fig. 2c). This image was taken on the region with a low surface density of Au catalyst to resolve the interface between graphene and a single CdS NW. It reveals that the CdS NW made a good contact with the graphene surface.

Fig. 2d shows the high-resolution transmission electron microscopy (HRTEM) image of an as-grown CdS NW. The distance between the lattice fringes was measured to be 0.25 nm, which was consistent with the *d*-spacing value of the {102} plane of wurtzite-structured CdS in the ICDD-PDF card (no. 41-1049). No obvious amorphous layer was observed on the surface of the NW, revealing the well-crystallized nature of our CdS NWs. This result clearly shows high-quality crystalline CdS NWs grown on the graphene surface.

The NWs were grown on the graphene for different time periods, and the relationship between the length of the NWs and their growth time was examined (Fig. 2e and S2 in the ESI†). When the growth time was short, only a partial region of the graphene was covered with short NWs (Fig. S2a in the ESI†). As the growth time increased, CdS NWs covered the entire graphene surface with catalyst, and the length of the grown NWs was found to be linearly proportional to the growth time (Fig. 2e).

In general, long NWs are expected to absorb more light than shorter ones because of their larger exposed surface area.[24] The dependence of the growth time of NWs on the sensitivity of the photoconductive channels was shown in Fig. 2e. In our works, the sensitivity was defined as a relative current difference $(I_{max} - I_{dark})/I_{dark}\%$, where I_{max} or I_{dark} represented the currents *with* or *without* a light source, respectively. Here, the light source was a xenon lamp (300 W), and a +0.1 V bias voltage was applied to the photoconductive channels. The sensitivity increased as the NW growth time increased up to 45 min (corresponding NW length ~4 μm), while it decreased when the growth time exceeded

45 min (Fig. 2e). Presumably, when the NWs were long (longer than ~4 μm in our case), some of the photo-generated carriers in the long NWs would recombine before reaching the graphene channel, which would be unfavorable for the transport and collection of the carriers. Thus in the following study, we utilized photoconductive channels including 4 μm long NWs grown for 45 minutes, which can provide an optimal device performance.

Photoresponse characteristics of photoconductive channels based on graphene–CdS NW hybrid structures

The photoconductivity of the channels based on graphene–CdS NW hybrid structures is shown in Fig. 3. For the measurement, we utilized the solar simulator (Newport 91160A) as a light source. This light source had a white light with a power density of 100 mW cm^{-2} (AM 1.5). All the photocurrent measurements were performed under the same conditions as previous photoconductivity experiments.[25] The inset in Fig. 3a shows typical *I–V* characteristics of our photoconductive channels with (red line) or without (black line) a light source. Fig. 3a shows the corresponding photocurrent ΔI which is defined as $I_{max} - I_{dark}$ at a specific bias voltage. The photocurrent ΔI was 2.60×10^{-2} mA, 9.08×10^{-2} mA and 4.42 mA at 0.1, 1.0 and 10 V bias voltages, respectively. The sensitivity $\Delta I/I_{dark}$ was estimated to be 25.6%, 8.9% and 42.4%, at 0.1, 1.0 and 10 V bias voltages, respectively. To avoid the geometry effect on photocurrent behavior, we have estimated the absolute photoresponsivity which could be calculated by ΔI/(*Light Receiving Area* × *Light Intensity*). The absolute photoresponsivity was 1.62 mA W^{-1}, 5.68 mA W^{-1} and 276 mA W^{-1} at 0.1, 1.0 and 10 V bias voltages, respectively. This absolute photoresponsivity of the channels based on graphene–CdS NW hybrid structures was higher than that of previously reported graphene-based channels.[17,19]

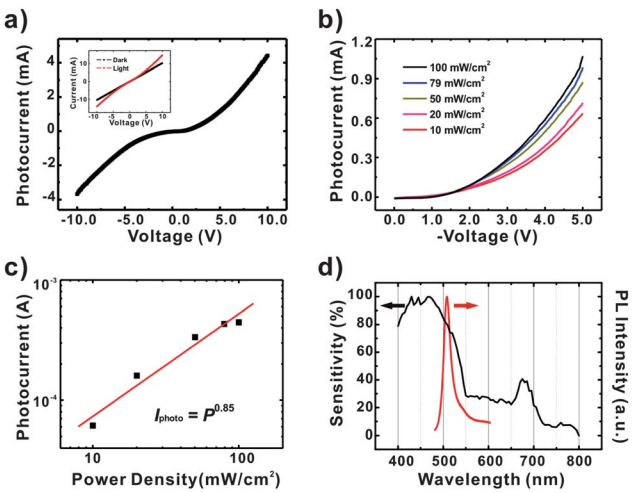

Fig. 3 Photoresponse of photoconductive channels based on graphene–CdS NW hybrid structures. (a) Photocurrent as a function of a bias voltage between the electrodes. The power of the light source was 100 mW cm^{-2}. The inset shows I–V characteristics with or without light exposure. (b) Photocurrent with various light power densities. (c) Graph showing the photocurrent as a function of light power density at a +3 V bias voltage. Note that the photocurrent is almost linearly proportional to the power density. (d) Spectral response (black line) of photoconductive channels at a constant bias +5 V and photoluminescence (PL) spectrum of graphene–CdS NW structures (red line). Note that a PL peak was observed near the wavelength (~516 nm) corresponding to the energy bandgap of CdS, and the spectral response also increased abruptly near the wavelength.

The absolute photoresponsivity behavior implies that the responsivity of the photoconductive channels based on graphene–CdS NW hybrid structures was larger than that of graphene-based channels,[17,19] while it was smaller than that of *individual* CdS NW or film-based channels.[2,12] However, the hybrid structure-based channels had a larger responsivity than CdS NW network-based channels.[8] This is because the CdS NW networks include a large empty area between individual NWs in the channel. Thus, the conductive channel area of the CdS NW *network*-based channels is smaller than that of the hybrid structures, which results in the low current level of the CdS NW networks.[8] For comparison, we fabricated *graphene*-based channels and *CdS NW network*-based channels with the same channel dimension as our hybrid structure channels and measured their photoresponsivity (Fig. S3 in the ESI†). It confirmed that the absolute photoresponsivity of photoconductive channels based on the hybrid structures was improved compared to that of graphene-based channels. Furthermore, the absolute responsivity of the photoconductive channels based on the hybrid structures was also higher than that of CdS NW network-based channels.

In the case of single-layer graphene, the lifetime of its photo-generated charge carriers is quite short (~picoseconds)[17,26] due to the ultrafast charge recombination process.[27] Therefore, the photocurrent generated by graphene could be negligible compared to that of CdS NWs in our hybrid structures. On the other hand, the graphene could be utilized as an efficient charge carrier-transport channel because of its superior electrical conductivity.[28,29] Thus, the photo-generated charge carriers in CdS NWs could be efficiently transported to the metal electrodes before their recombination. Also, it should be noted that other metals would not work as photoconductive channels because most of the metals already have a large amount of charge carriers and, thus, their conductivity would not change much unless extremely large amounts of photocurrents were generated by lights.[30–32] On the other hand, since the number of charge carriers in graphene was rather small, the photo-generated charge carriers in CdS NWs can significantly increase the carrier density in the graphene, and, thus, the graphene could work as a photoresponsive channel.[17,18]

Fig. 3b shows the photocurrent *versus* bias voltage with various optical power densities of the light source tuned by optical power filters. As expected, the amount of photocurrent increased as the optical power density increased. The photocurrent at a +3 V bias voltage was plotted as a function of incident optical power density in Fig. 3c. This photocurrent behavior could be fitted by a simple power law,[22,33]

$$I_p \approx AP^x$$

where I_p, A and P represent the photocurrent, the proportionality constant, and the optical power of the light source, respectively. Here, the exponent x is affected by the density of trap states between the Fermi level and the conduction band of the CdS NWs in our photoconductive channels.[22,34] Specifically,

when the trap state density is low, the photocurrent is linearly proportional to the power density of an incident light, and x should be close to 1. However, if the device channels have a rather large density of trap states, x should be much smaller than 1 because the trap states reduce the lifetime of the photogenerated carriers.[35] The fitting results of our photoconductive channels show $x = 0.85$, which is larger than the values of CdS nanoribbon-photodetectors[22] and, thus, indicates that the junctions between the graphene and CdS NWs in our device have a rather low density of trap states.

Fig. 3d depicts the spectral response (black line) and photoluminescence (PL, red line) of photoconductive channels based on graphene–CdS NW hybrid structures. For the measurement of the spectral response, a xenon lamp (300 W) and monochromator were used to provide the monochromatic light. With the monochromatic light of specific wavelengths, the sensitivity $\Delta I/I_{dark}$ of the photoconductive channels was measured at a +5 V bias voltage. The PL peak was found near the wavelength corresponding to the CdS bandgap energy (wavelength = 516 nm), indicating its band-edge emission nature.[22] Note that the sensitivity $\Delta I/I_{dark}$ of the photoconductive channels also increased rapidly near this wavelength. Here, the sensitivity was given in relation with the maximum sensitivity as 100% to clarify the spectral responsivity.[36] As expected, the sensitivity was quite small for the light with its wavelength longer than 550 nm, since the photons did not have enough energy to generate electron–hole pairs. When the wavelength of light source became shorter than 550 nm, the sensitivity increased rapidly and reached a maximum value near a wavelength of 460 nm. When the wavelength became shorter than 460 nm, the sensitivity decreased again because the photons of such energies were easily absorbed by other nearby structures.[35,36]

Time response characteristics of photoconductive channels based on graphene–CdS NW hybrid structures

A high-speed photoresponse is a crucial requirement for practical optoelectronic applications. Fig. 4 shows typical time response characteristics of photoconductive channels based on graphene–CdS NW hybrid structures. A xenon lamp (300 W) and a mechanical chopper were used to provide the intensity-modulated input light. During the measurement, +1 V bias voltage was applied onto the graphene channels. Fig. 4a and b depict the photocurrent responses to intensity modulations of 100 and 3000 Hz, respectively.

The photoconductive channels based on graphene–CdS NW hybrid structures responded up to 3000 Hz. The measured rise time t_r was 85 μs, and the fall time t_f was 140 μs. Here, we defined the *rise* time and the *fall* time as the time required for the current to *increase from 10% to 90% of* I_{max} and *decrease from 90% to 10% of* I_{max}, respectively. Note that even though these photoresponse and recovery speeds were slower than those of graphene-based photodetectors,[17] the speeds of our photoconductive channels were much faster than those of previously reported photoconductive channels based on CdS NW networks.[8] It implies that the graphene–CdS NW hybrid structure is a promising strategy to improve the performance of previous CdS NW *network-based* photodetectors. In addition, the 3 dB bandwidth, which is known to follow the relationship

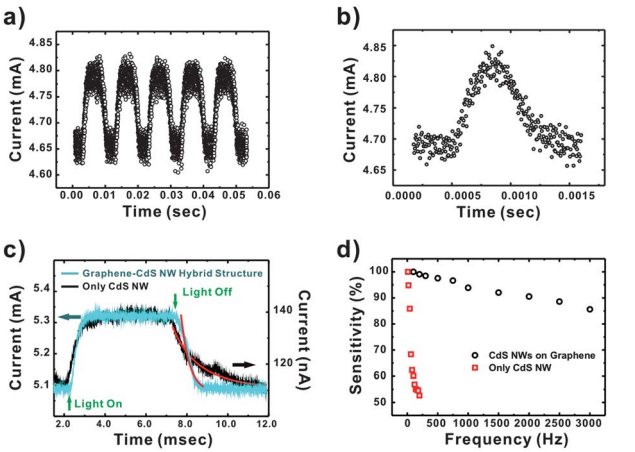

Fig. 4 Time response of photoconductive channels based on graphene–CdS NW hybrid structures. (a) Photoresponse and recovery of the photoconductive channels to the intensity-modulated light (100 Hz). (b) Photoresponse and recovery of the photoconductive channels to the high frequency light (3000 Hz). 3000 Hz was the highest input light frequency without severe deformation of the photocurrent signal. (c) Single modulation cycle of graphene–CdS NW hybrid structures (black) and only CdS NWs (blue) at 100 Hz-modulated light. Note that the hybrid structure shows a faster falling process compared to the conventional CdS NWs. (d) Frequency response of the photoconductive channels based on graphene–CdS NW hybrid structures and those based only on CdS NWs. The photoconductive channels based on graphene–CdS NW hybrid structures showed much wider bandwidth than CdS NW-based photoconductive channels.

$f_{3dB} = 0.35/t_r$, was estimated as 4.118 kHz for our photoconductive channels. This bandwidth is rather large compared to the previously reported bandwidth (~467 Hz) of CdS nanoribbon-based photodetectors.[22]

Fig. 4c shows typical response curves of the photoconductive channels based on graphene–CdS NW hybrid structures (black) and only CdS NWs (blue). In the case of the photoconductive channels based on only CdS NWs, the decay curve of the photocurrent can be fitted by the biexponential equation

$$I = I_0\left(Ae^{-\frac{t}{\tau_1}} + Be^{-\frac{t}{\tau_2}}\right)$$

as reported previously.[22] It indicates that there are two distinct processes in photocurrent decay. Previous works show that the recombination barrier occurred in rather thick NWs because the energy band bent upwards near the surface of the NWs due to Fermi-level pinning.[35] And, such a recombination barrier would result in a slow decay process in the NWs.[22,35] On the other hand, the photoconductive channels based on graphene–CdS NW hybrid structures showed a mono-exponential decay behavior such as

$$I = I_0\left(Ae^{-\frac{t}{\tau}}\right),$$

and this decay process was much faster than that of the photoconductive channels based on only CdS NWs. In the case of the CdS NWs, the time constant for the fast decay τ_1 and slow decay τ_2 were observed to be 750 μs and 1.53 ms, respectively. However, the decay time constant for the photoconductive channel based on graphene–CdS NW hybrid structures was about 130 μs.

Presumably, since photocarriers generated in CdS NWs have to flow through the graphene channels, the highly conductive graphene channel could induce a rapid decay process.

Fig. 4d shows the sensitivity $\Delta I/I_{dark}$ of the photoconductive channels *versus* the frequency of an incident light signal. The *black circles* and the *red squares* show the sensitivity of the photoconductive channel based on *graphene–CdS NW hybrid structures* and that based on *CdS NWs*, respectively. Here, the sensitivity was given in relative units, where the maximum sensitivity was considered as 100% sensitivity.[36] Our measured results show the photoconductive channels based on the graphene–CdS NW hybrid structures could operate even at a high frequency (up to 3000 Hz) unlike photoconductive channels based on only CdS NWs. It clearly shows that the photoconductive channels based on graphene–CdS hybrid structures had much broader 3 dB bandwidth than those based on only CdS NWs.

Conclusions

In summary, we have developed a high-performance photoconductive channel based on graphene–CdS NW hybrid structures which takes advantages of both graphene and semiconducting NWs. The responsivity of the photoconductive channel was much larger than that of previously reported graphene-based photoconductive channels. Furthermore, our photoconductive channels exhibited much faster decay process than previous photoconductive channels based on CdS NW networks, which resulted in fast sensor speed and wide bandwidth. Such a fast decay process was attributed to the fast decay of photocarriers in graphene channels. This simple but efficient strategy should allow us to build high-speed optoelectronic devices for practical applications.

Acknowledgements

This work was supported by the NRF grant (no. 2011-0000390) and the NBIT program. S. H. acknowledges the financial support from the WCU program (no. R31-10032) and the Conversing Research Center Program (no. 2011K000683). J. J. acknowledges the financial support from the China–Korea Young Scientist Exchange program and NSFC grant (no. 50862008). K. S. K. acknowledges the financial support from NRF (National Honor Scientist Program, no. 2010-0020414). B. H. H. acknowledges the financial support from Basic Science Research Program (no. 2011-0017587).

Notes and references

1 M. A. Khan, J. N. Kuznia, D. T. Olson, M. Blasingame and A. R. Bhattarai, *Appl. Phys. Lett.*, 1993, **63**, 2455.
2 D. P. Amalnerkar, *Mater. Chem. Phys.*, 1999, **60**, 1.
3 V. M. Garcia, M. T. S. Nair, P. K. Nair and R. A. Zingaro, *Semicond. Sci. Technol.*, 1996, **11**, 427.
4 J. Dresner and F. V. Shallcross, *J. Appl. Phys.*, 1963, **34**, 2390.
5 T. Gao, Q. H. Li and T. H. Wang, *Appl. Phys. Lett.*, 2005, **86**, 173105.
6 X. G. Peng, L. Manna, W. D. Yang, J. Wickham, E. Scher, A. Kadavanich and A. P. Alivisatos, *Nature*, 2000, **404**, 59.
7 S. C. Kung, W. E. van der Veer, F. Yang, K. C. Donavan and R. M. Penner, *Nano Lett.*, 2010, **10**, 1481.
8 G. S. Paul and P. Agarwal, *J. Appl. Phys.*, 2009, **106**, 103705.
9 H. F. Bao, C. M. Li, X. Q. Cui, Q. L. Song, H. B. Yang and J. Guo, *Nanotechnology*, 2008, **19**, 335302.
10 Y. J. Choi, K. S. Park and J. G. Park, *Nanotechnology*, 2010, **21**, 505605.
11 C. Y. Yan, N. Singh and P. S. Lee, *Appl. Phys. Lett.*, 2010, **96**, 053108.
12 Y. Ye, L. Dai, X. N. Wen, P. C. Wu, R. M. Pen and G. G. Qin, *ACS Appl. Mater. Interfaces*, 2010, **2**, 2724.
13 L. Li, P. C. Wu, X. S. Fang, T. Y. Zhai, L. Dai, M. Y. Liao, Y. Koide, H. Q. Wang, Y. Bando and D. Golberg, *Adv. Mater.*, 2010, **22**, 3161.
14 Q. G. Li and R. M. Penner, *Nano Lett.*, 2005, **5**, 1720.
15 T. Zhai, L. Li, X. Wang, X. S. Fang, Y. Bando and D. Golberg, *Adv. Funct. Mater.*, 2010, **20**, 4233.
16 Y. Jiang, W. J. Zhang, J. S. Jie, X. M. Meng, X. Fan and S. T. Lee, *Adv. Funct. Mater.*, 2007, **17**, 1795.
17 F. N. Xia, T. Mueller, Y. M. Lin, A. Valdes-Garcia and P. Avouris, *Nat. Nanotechnol.*, 2009, **4**, 839.
18 T. Mueller, F. N. A. Xia and P. Avouris, *Nat. Photonics*, 2010, **4**, 297.
19 Y. M. Shi, W. J. Fang, K. K. Zhang, W. J. Zhang and L. J. Li, *Small*, 2009, **5**, 2005.
20 K. S. Kim, Y. Zhao, H. Jang, S. Y. Lee, J. M. Kim, K. S. Kim, J. H. Ahn, P. Kim, J. Y. Choi and B. H. Hong, *Nature*, 2009, **457**, 706.
21 Y. Lee, S. Bae, H. Jang, S. Jang, S. E. Zhu, S. H. Sim, Y. I. Song, B. H. Hong and J. H. Ahn, *Nano Lett.*, 2010, **10**, 490.
22 J. S. Jie, W. J. Zhang, Y. Jiang, X. M. Meng, Y. Q. Li and S. T. Lee, *Nano Lett.*, 2006, **6**, 1887.
23 Y. W. Wang, G. W. Meng, L. D. Zhang, C. H. Liang and J. Zhang, *Chem. Mater.*, 2002, **14**, 1773.
24 C. Soci, A. Zhang, X. Y. Bao, H. Kim, Y. Lo and D. L. Wang, *J. Nanosci. Nanotechnol.*, 2010, **10**, 1430.
25 R. X. Yan, D. Gargas and P. D. Yang, *Nat. Photonics*, 2009, **3**, 569.
26 P. A. George, J. Strait, J. Dawlaty, S. Shivaraman, M. Chandrashekhar, F. Rana and M. G. Spencer, *Nano Lett.*, 2008, **8**, 4248.
27 J. M. Dawlaty, S. Shivaraman, M. Chandrashekhar, F. Rana and M. G. Spencer, *Appl. Phys. Lett.*, 2008, **92**, 042116.
28 K. S. Novoselov, A. K. Geim, S. V. Morozov, D. Jian, M. I. Katsnelson, I. V. Grigorieva, S. V. Dubonos and A. A. Firsvo, *Nature*, 2005, **438**, 197.
29 A. N. Cao, Z. Liu, S. S. Chu, M. H. Wu, Z. M. Ye, Z. W. Cai, Y. L. Chang, S. F. Wang, Q. H. Gong and Y. F. Liu, *Adv. Mater.*, 2010, **22**, 103.
30 S. G. Hickey and D. J. Riley, *J. Phys. Chem. B*, 1999, **103**, 4599.
31 L. H. Laih, T. C. Chang, Y. A. Chen, W. C. Tsay and J. W. Hong, *IEEE Photonics Technol. Lett.*, 1998, **10**, 579.
32 T. Nakanishi, B. Ohtani and K. Uosaki, *J. Phys. Chem. B*, 1998, **102**, 1571.
33 H. Kind, H. Q. Yan, B. Messer, M. Law and P. D. Yang, *Adv. Mater.*, 2002, **14**, 158.
34 A. Rose, *Concepts in Photoconductivity and Allied Problems*, Rev. ed. Krieger, New York, US, 1978, p xii, 168 p.
35 R. Calarco, M. Marso, T. Richter, A. I. Aykanat, R. Meijers, A. V. Hart, T. Stoica and H. Luth, *Nano Lett.*, 2005, **5**, 981.
36 N. V. Joshi, *Photoconductivity: Art, Science, and Technology*, M. Dekker, New York, US, 1990, p x, 309 p.

